# Size-Controlled Growth of Germanium Nanowires from Ternary Eutectic Alloy Catalysts

*Colm O'Regan*[†,ϕ], *Subhajit Biswas*[†,ϕ], *Sven Barth*[§], *Michael A. Morris*[†,ϕ], *Nikolay Petkov*[†,ϕ] *and Justin D. Holmes*[†,ϕ,*]

[†]*Materials Chemistry & Analysis Group, Department of Chemistry of the Tyndall National Institute, University College Cork, Ireland.* [ϕ]*Centre for Research on Adaptive Nanostructures and Nanodevices (CRANN), Trinity College Dublin, Dublin 2, Ireland.* [§]*Institute for Materials Chemistry, Vienna University of Technology, A-1060 Vienna, Austria.*

*To whom correspondence should be addressed: Tel: +353 (0)21 4903608; Fax: +353 (0)21 4274097; E-mail: j.holmes@ucc.ie

## Abstract

We report the size-controlled growth of Ge nanowires from Au-Ag-Ge ternary alloy catalysts. Significantly, Au-Ag-Ge layered thin films enabled, for the first time, the synthesis of high aspect ratio Ge nanowires by simultaneously manipulating both the solute concentration ($C$) and equilibrium concentration ($C_{eq}$) of Ge in the catalysts, thereby increasing the Ge supersaturation during vapour-liquid-solid (VLS) growth. Simultaneous manipulation of $C$ and $C_{eq}$ to enhance nanowire growth rates was also achieved using colloidal $Au_{0.75}Ag_{0.25}$ nanoparticles deposited on a Ge film. These nanoparticles produced Ge nanowires with more uniform diameter distributions than those obtained from the thin films. The manifestation of the Gibbs-Thomson effect, resulting in a diameter dependent growth rate, was observed for all nanowires grown from $Au_{0.75}Ag_{0.25}$

nanoparticles. In-situ TEM heating experiments performed on the as-grown Ge nanowires enabled direct determination of the Ge equilibrium concentrations in the Au-Ag-Ge ternary alloys.

**Keywords:** Germanium, nanowires, vapour-liquid-solid, ternary alloy, supersaturation, growth kinetics

## Introduction

Germanium nanowires are regarded as promising materials for a number of applications, including nanoelectromechanical systems [1, 2], lithium-ion batteries [3-5] and field-effect transistors [6]. However, such devices require nanowires with consistent and reproducible dimensions, *e.g.* length and diameter. Tailoring nanowire dimensions by manipulating their vapour-liquid-solid (VLS) growth kinetics, allows the synthesis of micrometre and even millimetre-long nanowires with uniform diameters. During the VLS growth process, supersaturation acts as the driving force for layer-by-layer crystallisation at the triple phase boundary (TPB).[7] Assuming the crystallisation of Ge nanowires is rate limiting, the enhanced rate of nanowire growth can be achieved by increasing the supersaturation of Ge in the eutectic alloy system. Tailoring the supersaturation of an alloy seed can be done by controlling either the equilibrium concentration ($C_{eq}$) or solute concentration ($C$) of the semiconductor material in the eutectic alloy system, according to equation 1 [8]:

$$\Delta\mu = kT\ln\left(\frac{C}{C_{eq}}\right) \quad (1)$$

where $\Delta\mu$ is the supersaturation of Ge in the binary alloy, $k$ is Boltzmann's Constant and $T$ is temperature. Supersaturation ($\Delta\mu$) of Ge in a eutectic growth system can be raised by increasing $C$ and/or decreasing $C_{eq}$. Manipulation of the supersaturation to influence GaAs nanowire growth has

been accomplished by Han *et al.* [9] by tuning the concentration of the growth species (solute concentration, *C*) during nanowire growth. Control over supersaturation, by varying the solute concentration in eutectic Au-Ga alloy seeds, was also achieved by altering the thickness of Au films used to seed nanowires. Additionally, we have previously reported the manipulation of solute concentration (*C*), and thus the supersaturation of Ge in Au-Ge alloy systems, by using Au-Ge bi-layer films as an alternative to pure Au films for synthesising Ge nanowires [10]. Increasing the thickness of the Ge layer resulted in an increase in the supersaturation, yielding elevated nanowire growth rates and lengths.

Another approach to increase the supersaturation ($\Delta\mu$) of Ge in the Au-Ge system, to influence nanowire growth kinetics, is to lower the equilibrium concentration, $C_{eq}$ of Ge in the liquid eutectic alloy (according to equation 1). A feasible way to manipulate $C_{eq}$ is to incorporate a foreign element into the collector phase, *i.e.* the metal seed particle, which can shift the liquidus phase boundary of the growth species towards a lower equilibrium concentration. Perea *et al.* adopted this approach by introducing Ga into Au seeds forming Au-Ga alloy particles for promoting nanowire growth[11]. With a Ga-Au ratio of 1:1, $C_{eq}$ was reduced by more than 6 times its original value, enabling the formation of very abrupt Si-Ge heterojunctions. For the Au-Ge binary alloy system, Ag is a preferred choice as a foreign element as it is completely miscible with Au, does not form intermetallic compounds and the bimetallic system of $Au_xAg_{1-x}$ forms a low temperature eutectic with Ge. Biswas *et al.*[12, 13] and Chou *et al.*[14] have employed Ag in Au-Ge eutectic systems to synthesise Ge nanowires. In particular, Biswas *et al.* used Ag to successfully lower $C_{eq}$ of Ge in a Au-Ge system to produce millimetre-long Ge nanowires[13]. Another bi-metallic catalyst system which has been used to seed nanowire growth is Au-Al (specifically, $AuAl_2$ seeds)[15]. In this case, the low solubility of Ge in the alloy seed resulted in the growth of ultra-sharp Si-Ge heterostructure interfaces. Ternary alloys of Ge have also been investigated for several systems[16-19], suggesting their potential as future growth

promoters of one-dimensional nanostructures. Moreover, the use of ternary alloys may allow doping of nanowires through the alloy seed particle[20], ensuring the incorporation of dopants into the lattice of a nanowire instead of along the sidewalls.

Eutectic point depression and the change in the Ge liquidus content due to nanoscale size effects[21] should also be considered for nanowire growth systems. Several groups have investigated nanoscale Au-Ge systems via in-situ temperature studies inside a transmission electron microscope (TEM)[8, 21-26]. These studies make use of, and expand upon, the nanoscale phase diagram of the Au-Ge system which was established by Sutter *et al.*[27, 28] and which compares the eutectic behaviour of the nanosystem to its bulk counterpart.

In this article, we report the successful combination of the two approaches of increasing the Ge solute concentration and decreasing the Ge equilibrium concentration in the Au-Ag-Ge ternary alloy system, to enhance nanowire growth kinetics through the use of tri-layer films. The manipulation of both $C$ and $C_{eq}$ through the use of $Au_xAg_{1-x}$ nanoparticle seeds and a Ge reaction layer (instead of using Au and Ag films) to produce long Ge nanowires with uniform diameters is also discussed. Finally, the established Gibbs-Thomson relationship and in-situ TEM heating experiments are used to explain the nanoscale size effects, *i.e.* diameter-dependent nanowire lengths for the ternary eutectic systems.

## Experimental

### Evaporation of thin films

Au, Au-Ag and Au-Ag-Ge films (Au = 10 nm, Ag = 3 nm, Ge = 4 or 6 nm) were evaporated onto $Si/SiO_2$ substrates (the $SiO_2$ layer was 200 nm) using a Temescal FC2000 e-beam evaporation system. The substrates were first treated with a 30 s in-situ Ar ion etch to improve adhesion. The

metals were then evaporated at a rate of 1 Å $s^{-1}$ with a quartz thickness monitor being used to carefully control the thickness of the films.

**Synthesis of Au and $Au_{0.75}Ag_{0.25}$ nanoparticles**

Au and $Au_{0.75}Ag_{0.25}$ nanoparticles used as growth promoters were prepared using a method outlined previously by Liu *et al.* [29]. Briefly, 0.3 mmol of $HAuCl_4.3H_2O$ (for Au nanoparticles) and 0.225 mmol of $HAuCl_4.3H_2O$ with 0.075 mmol of silver acetate (for $Au_{0.75}Ag_{0.25}$ nanoparticles) were mixed with 2 ml oleylamine, 1 ml oleic acid and 10 ml phenyl ether under an Ar atmosphere and heated to 150 °C with constant stirring. The solutions were kept at that temperature for 4 hr and then cooled to room temperature. Nanoparticles were precipitated and cleaned with ethanol and dispersed in toluene for further use as catalysts for nanowire growth.

**Synthesis of Ge nanowires from thin films and colloidal nanoparticles**

Continuous-flow reactions were carried out in a toluene medium by liquid injection chemical vapour deposition (LICVD). The substrates were loaded into a stainless steel micro reactor cell connected by metal tubing. The reaction cell and connections were dried for 24 hr at 180 °C under vacuum after which the diphenylgermane (DPG) precursor solution was loaded into a Hamilton GASTIGHT[R] syringe [1000 series] with a luer lock inside a $N_2$ filled glovebox. Solutions of diphenylgermane (DPG) in anhydrous toluene were prepared in an $N_2$ glove box with a typical concentration of $1.07 \times 10^{-4}$ M. Prior to injection, the substrate was annealed for 30 min at 465 °C under a flowing $H_2$/Ar atmosphere inside a tube furnace. The precursor solution was then injected into the metal reaction cell using a high precision syringe pump at a rate of 0.025 ml $min^{-1}$. A $H_2$/Ar flow, with a flow rate of 0.5 ml $min^{-1}$, was maintained during the entire growth period. This setup is shown schematically in figure 1. Typical growth times were 30 min. The cell was allowed to cool

to room temperature and disassembled to access the growth substrate. Nanowires were washed with dry toluene and dried under $N_2$ for further characterisation.

For the particle seeded growth, Au and $Au_{0.75}Ag_{0.25}$ particles were drop-cast onto $SiO_2$/Si substrates coated with 6 nm of evaporated Ge. Ge thin film-coated substrates were pre-treated by dipping in a 1 % HF solution for 30 s to remove the native $GeO_2$ layer. The particle solutions were then drop-casted onto the substrate and dried under nitrogen. Nanoparticle-coated substrates were placed inside a stainless steel micro reactor cell attached with high precision needle valves. The synthesis was carried out as described above for tri-layer films.

**Characterisation**

Scanning electron microscopy (SEM) analysis was undertaken on a FEI Quanta FEG 650 operating at 5-10 kV. High-resolution phase-contrast transmission electron microscopy (TEM), in-situ temperature dependent studies and selected area electron diffraction (SAED) were carried out on a JEOL JEM 2100F transmission electron microscope operating at 200 kV, while energy dispersive X-ray (EDX) analysis was carried out using an Oxford Instruments INCA energy system fitted to the TEM. UV-visible absorbance spectroscopy of the Au and $Au_{0.75}Ag_{0.25}$ particles was carried out using an Agilent Technologies Varian Cary 50 UV-Vis spectrophotometer. For TEM characterisation, nanowires were dispersed in isopropanol via sonication and dropped onto lacey carbon 400 mesh copper grids. Nanowire lengths and diameters were determined by TEM and scanning transmission electron microscopy (STEM).

## Results

### Ge nanowire growth from three-part film substrate

Our experiments consisted of utilising a 3-part substrate (shown in figure 1) to grow Ge nanowires. The substrate consisted of a Au film, a Au-Ag bi-layer and a Au-Ag-Ge tri-layer. Figure 2 shows SEM images of Ge nanowires grown from each of the three sections of the substrate. Nanowires grown from the Au film (10 nm), Au-Ag bi-layer (10 nm-3 nm) and the Au-Ag-Ge tri-layer (10 nm-3 nm-6 nm) are shown in figures 2(a), (b) and (c) respectively. Nanowires with broad diameter distributions were synthesised from the Au and Au-Ag sections of the substrate (figures 2(a) and (b)) with mean diameters of 80.2 ± 37 nm and 100.5 ± 66 nm respectively. The Au-Ag-Ge tri-layer showed a clear bimodal distribution in radial dimensions with a mean diameter of 265 ± 148 nm for the thicker regime and a mean diameter of 41 ± 11 nm for the thinner nanowires (figure 2 (c) inset). Figure 2(d) compares the nanowire length distributions, with the mean lengths increasing progressively from 2.0 ± 0.9 μm for the Au film to 5.0 ± 4.2 μm for the Au-Ag bi-layer and finally, to 7.3 ± 4.3 μm for the Au-Ag-Ge tri-layer (Ge layer is 6 nm). Figures S1(a) and (b) (see Supporting Information) shows SEM images of Ge nanowires grown from Au-Ge binary and Au-Ag-Ge ternary alloys respectively and confirms (via cross-sectional SEM imaging 90 degrees to the beam) that longer nanowires were synthesised from the ternary alloys. Thus, adding a Ag layer to the conventional Au film (Au-Ag bi-layer and Au-Ag-Ge tri-layer) produced longer nanowires than standard Au seeded nanowire growth. Figures S1(a) and (b) also highlight the broad diameter distribution for Ge nanowires synthesised from the 3-part substrate. Figures S1(c), (d) and (e) (see Supporting Information) show high-resolution phase-contrast TEM micrographs of typical nanowires grown on all 3 sections of the substrate. Monocrystalline Ge was confirmed with a [111] growth orientation for all of the nanowires analysed by SAED. These nanowires were representative of the majority of the nanowires grown on the 3-part substrates, with negligible differences in structure and orientation between the Au film, the Au-Ag bi-layer and the Au-Ag-Ge tri-layer.

Figure S2 shows a high-angle-annular-dark-field (HAADF) STEM image of one such nanowire grown on the Au-Ag-Ge side of the substrate. The EDX scans confirmed the presence of both Ag (24.6 %) and Au (75.4 %) in the seed particle.

**Ge Nanowire growth from nanoparticles with a Ge reaction layer**

Figure S3(c) shows an SEM image of a Au-Ag-Ge film after annealing for 30 min at 465 ºC and clearly highlights a bimodal distribution in particle diameters. Ge nanowires were subsequently grown from these particles, thus also giving a bimodal distribution in nanowire diameters (265.4 ± 148 nm and 41.3 ± 11 nm), as seen in figure 2(c). Note that while there exists a broad size distribution with nanowires grown from the Au film and Au-Ag bi-layer, there is no obvious bi-modal regime observed from the SEM images (figures 2(a) and (b)). The inset in figure 2(c) is a plot of the diameter distribution, confirming the bimodal diameter regime in the nanowires. To yield nanowires with a more uniform diameter distribution, we synthesised Ge nanowires from monodisperse $Au_xAg_{1-x}$ nanoparticles (shown in figure 2(e)) deposited on a Ge film (6 nm thickness). The nanoparticles had a mean diameter of 13.9 ± 1.9 nm. A single surface plasmon resonance (SPR) peak observed in the absorbance spectra (figure S3(d), Supporting Information) confirmed the formation of a Au-Ag alloy instead of two different phases of Ag and Au in the sample. A blue shift of the SPR peak from similar sized Au nanoparticles (TEM image shown in figure S3(a), Supporting Information) also confirmed the formation of Au-Ag alloy nanoparticles[29]. The Ge nanowires that were grown from these $Au_xAg_{1-x}$ seeds are shown in figure 2(f). The SEM image and corresponding inset of the nanowire diameter distribution revealed the absence of a bimodal regime, with highly uniform diameters. The mean diameter of the Ge nanowires grown from the alloy nanoparticle seeds was 44.2 ± 14 nm, which was much smaller than the mean diameter obtained from the evaporated films. The atomic percentage of Au and Ag at the metal tips of the nanowires (see figure S4, Supporting Information) was confirmed by EDX analysis (72.3 at%

Au and 27.7 at% Ag) and it should be noted that this composition is nearly identical to the composition of the Au-Ag metal tip at the end of the nanowires grown from the Au-Ag-Ge trilayer films (figure S2, Supporting Information). To compare the growth kinetics of $Au_xAg_{1-x}$ seeded Ge nanowires with phase pure Au seeded nanowires, we also used colloidal Au nanoparticles to seed Ge nanowire growth (figures S3(a) and (b), Supporting Information) for a comparison of the length scale between the two different seeds.

## Discussion

### Utilisation of Ag film to reduce equilibrium concentration of Ge

Figure 3(a) displays the partial phase diagram of the Au-Ge and $Au_{0.75}$-$Ag_{0.25}$-Ge system [30, 31] and shows how adding Ag to the Au-Ge binary system shifts the Ge-liquidus curve towards lower equilibrium concentrations [13]. The black line in figure 3(a) represents the liquidus curve for the Au-Ge binary system. At a growth temperature of 465 ºC, the equilibrium concentration ($C_{eq}$) of Ge in the Au-Ge binary eutectic alloy was approximately 35 at.%. The red line represents the liquidus curve for the $Au_{0.75}$-$Ag_{0.25}$-Ge ternary alloy system. Addition of Ag to the Au-Ge binary system reduces $C_{eq}$ for a given temperature (22 at.% at the growth temperature of 465 ºC) with a moderate change in the eutectic temperature, thus suggesting higher supersaturation ($\Delta\mu$) of Ge in the eutectic alloy (according to equation 1) for the ternary eutectic system. As a consequence of the higher supersaturation, the nanowire growth rate increases and yields longer nanowires according to the growth model proposed by Givargizov [32]; as shown in equation 2:

$$v = b\left(\frac{\Delta\mu}{kT}\right)^2 \qquad (2)$$

where $v$ is the growth rate and $b$ is the kinetic coefficient of crystallisation. We have considered the $Au_{0.75}$-$Ag_{0.25}$-Ge (*ie.* 75 % Au and 25 % Ag) binary phase diagram to explain the nanowire growth scenarios with the Au-Ag-Ge tri-layer films, as the atomic ratio of Ag (23 at %) in the bi-layer film (10 nm Au - 3 nm Ag) estimated from the Au and Ag film thickness nearly matches with the $Au_{0.75}Ag_{0.25}$ system. Also, EDX studies confirmed the presence of Ag and Au in the growth seeds with a 1:3 ratio (see figure S2, Supporting Information). Length distributions of nanowires grown from Au and Au-Ag bi-layer films, shown in figure 3(b), suggest that $C_{eq}$ of Ge is considerably lowered in the Au-Ag alloy seeds. An increase in the mean length of the nanowires from 2.0 ± 0.9 μm for the Au seeds to 5.0 ± 4.2 μm with the Au-Ag alloy is due to the enhanced supersaturation of Ge within the Au-Ag alloy seeds, resulting in fast nanowire growth.

Nanowire crystallisation was faster at the triple phase interface for the Au-Ag section of a substrate compared to the Au section. As the Ge vapour concentration is similar for all experiments, the chemical potential gradient of Ge between the vapour phase and liquid phase will depend on $C_{eq}$ of each system. This driving force (difference in the chemical potential between the vapour and liquid phases) for Ge absorption into the catalyst seeds will be different for each catalyst system; greater absorption of Ge would be expected in the Au-Ag catalyst compared to Au. Although measuring the transient Ge concentration ($C$) in the catalysts is beyond the scope of the experiments performed in this study, we have assumed that the Au-Ag system will have higher ($C$-$C_{eq}$) values than the Au system ($C$ is the transient or solute concentration), which will also contribute towards a higher supersaturation in the Au-Ag seeds.

Finally, figure S5 in the Supporting Information shows nanowire growth from a Au-coated substrate (no Ag or Ge films present). The SEM images show nanowire growth on the left, middle and right portions of the substrate and reveal that growth was consistent across the entire substrate.

Nanowires did not grow faster on the left side of the substrate when compared to the middle or right side, suggesting that the catalyst is the dominant factor in determining nanowire growth kinetics on the 3-part substrates.

**Utilisation of Ge film to increase solute concentration of Ge**

Figure 4(a) shows nanowire length distributions for Au-Ag-Ge tri-layer sides of two substrate with different Ge layer thicknesses. The distribution reveals longer nanowires for the 6 nm Ge film when compared to a 4 nm film (mean lengths of 7.5 ± 4.3 μm and 5.7 ± 2.3 μm respectively). Adding Ge to Au-Ag films creates Au-Ag-Ge ternary eutectic alloy particles upon annealing before the subsequent introduction of a Ge precursor. Consequently, this raises the Ge solute concentration (*C*) in the Au-Ag-Ge system which in turn increases the supersaturation according to equation 1, as detailed in our previous report[10]. Briefly, increasing the solute concentration of Ge in the alloy seed is associated with increasing the chemical potential of the growth species, thus increasing the driving force responsible for nanowire growth. Increasing the solute concentration through the addition of Ge films is equivalent to increasing the partial pressure of a vapour source, which has been previously performed[8] to increase the supersaturation of Ge. When the Ge precursor is introduced, the incubation time for Ge nucleation (and thus nanowire growth) to occur is therefore lessened according equation 3 below [22]:

$$\tau = \exp\left(\frac{b}{\Delta\mu^2}\right) \qquad (3)$$

where $\tau$ is the incubation time for growth. Figure 4(b) shows an enhancement of the eutectic region of the phase diagrams of the Au-Ge binary (black line) and $Au_{0.75}$-$Ag_{0.25}$-Ge ternary (red line) systems [30, 31] and traces the progression of the physical behaviour of a $Au_{0.75}$ -$Ag_{0.25}$ -Ge ternary alloy

system as the concentration of Ge in the alloy increases. The red line represents the Ge liquidus of the $Au_{0.75}$-$Ag_{0.25}$-Ge system and is shifted towards a reduced equilibrium concentration as a result of incorporating Ag into the Au-Ge alloy. Further addition of a Ge film helps to pre-form Au-Ag-Ge ternary eutectic alloy particles during the annealing stage prior to nanowire growth. The annealing process creates ternary alloy catalyst melts only on the Au-Ag-Ge side of the substrate, which participate as the promoters in the nanowire growth process. For a pure Au or Au-Ag film, there is no Ge present and so the system remains on the far left of the phase diagram (0 % Ge). Assuming the absence of a Ge precursor, the Au and Au-Ag films do not form a eutectic alloy upon annealing at the growth temperature prior to the actual nanowire growth. On the Au-Ag-Ge side, the introduction of a 4 nm Ge film (21.3 at.% Ge) in the Au/Ag system, places the ternary alloy system at point (i) (marked with a blue arrow in figure 4(b)) on the phase diagram. The Ge layer places the ternary alloy system extremely close to the equilibrium concentration for the $Au_{0.75}$-$Ag_{0.25}$-Ge system, $C_{eq}$ (marked by the red arrow). A further increase in the Ge film thickness to 6 nm, which corresponds to 29 at.% Ge in Au/Ag alloy, places the solute concentration above $C_{eq}$ of Ge, (point (ii) in figure 4(b)) resulting in a drastically reduced incubation time for nucleation (due to the increase in supersaturation). The reduced incubation time for Ge nanowire growth with the thicker (6 nm) Ge layer is reflected in the experimental data shown in figure 4(a), with longer nanowires being generated from a 6 nm Ge film compared to a 4 nm film. Along with the reduction of incubation time, the Ge reaction layer in the tri-layer film also enhances the actual solute concentration in the catalyst and hence the supersaturation. The enhanced Ge adatom concentration around the catalyst seed with the extra Ge buffer layer will increase the transient Ge concentration in the seed during nanowire growth. Importantly, the Au-Ag-Ge tri-layer section of the substrate makes use of both a Ag and Ge film, which allows the simultaneously manipulation of both the solute concentration ($C$) and equilibrium concentration ($C_{eq}$) of Ge in the ternary alloy seeds.

**Ge nanowire growth from $Au_xAg_{1-x}$ nanoparticles and the Gibbs-Thomson effect**

As shown in figure 2(c), a bi-modal diameter distribution was obtained for Ge nanowires grown from the Au-Ag-Ge tri-layer portion of our substrate. An in-depth study on the formation of the bi-modal diameter distributions is beyond the scope of this work and will be required to conclusively determine the exact method by which it forms. However, regardless of the mechanism of formation, bimodal diameters are generally undesirable due to the drastic differences in the Ge nanowire properties that inevitably result from such a large difference in radial dimensions. Additionally, the diameters of the nanowires obtained from the Au films and Au-Ag bi-layers were quite pronounced (mean wire diameters were approximately 80 and 100 nm respectively, figures 2(a) and (b)). These large nanowire diameters are likely a result of Ostwald ripening due to surface diffusion of atoms at the relatively high temperature of 465 ºC [33, 34]. Consequently, experiments to remove the bimodal distribution to produce nanowires with more uniform diameters and to yield thin nanowires with high aspect ratios were undertaken using monodisperse colloidal nanoparticles (instead of evaporated films). The growth of Ge nanowires from these nanoparticles was accomplished by drop-casting $Au_{0.75}Ag_{0.25}$ alloy particles and Au particles onto $Si/SiO_2$ substrates that were coated with 6 nm of evaporated Ge (figures 2(e) and (f), figure S3(a) and (b)). This combination of using a Ge layer with $Au_{0.75}Ag_{0.25}$ nanoparticles enabled both the equilibrium concentration (by using the Au-Ag alloy nanoparticles) and the solute concentration (by dropping casting the nanoparticles onto Ge films; the films acted as a source of Ge before the precursor is injected) was undertaken.

Figure 5(a) shows a comparison of the length distributions of nanowires synthesised from size-monodisperse Au nanoparticles deposited on a bare $SiO_2$ substrate (2.3 ± 0.9 μm), nanowires synthesised from Au nanoparticles deposited on a 6 nm Ge film (4.4 ± 1.7 μm) and nanowires grown from $Au_{0.75}Ag_{0.25}$ nanoparticles deposited on a 6 nm Ge film (8.7 ± 5.2 μm). The increase in length from 2.3 ± 0.9 μm for Au-nanoparticle seeded Ge nanowires to 4.4 ± 1.7 μm for Au-film seeded

growth with a Ge buffer layer, confirms the participation of the Ge film in the growth process; by increasing the Ge solute concentration in the Au-Ge alloy and hence positively influencing Ge supersaturation. The further increase in the nanowire length to 8.7 ± 5.2 μm for nanowires synthesised from $Au_{0.75}Ag_{0.25}$ seeds deposited on a 6 nm Ge layer is due to a reduction in the Ge equilibrium concentration ($C_{eq}$) as a result of adding Ag to the Au-Ge system, along with the increase in the solute concentration, due to the Ge buffer layer. The growth rates and lengths of the nanowires grown from the Au, Au-Ag and Au-Ag-Ge evaporated films (figures 2(a), (b) and (c)), as well as those nanowires grown from the Au and $Au_{0.75}Ag_{0.25}$ nanoparticles (figure S3(b) and figure 2(f)), are summarised in table 1. The table identifies the system which yields the highest growth rate and longest nanowires as the $Au_{0.75}Ag_{0.25}$ nanoparticles deposited on 6 nm Ge buffer layers. This 6 nm buffer layer on the $SiO_2$ substrate is acting in two different ways to enhance the nanowire growth kinetics. Firstly, the Ge layer is actively increasing the Ge adatom concentration surrounding the catalyst and hence increasing the transient (solute) concentration of Ge during nanowire growth. Increasing the solute concentration in the catalyst using a Ge layer will increase $\Delta\mu$ (according to equation 1) and hence the nanowire growth rate (according to equation 2). As well as increasing the transient Ge concentration, the Ge reaction layer also participates in reducing the incubation time for Ge nucleation by pre-forming a eutectic melt at the growth temperature.

Ideally, nanowire growth times should be separated into the constituent components of incubation time, *i.e* the time required for the initial nucleation ($T_N$) to take place from precursor injection and the time of actual growth ($T_G$). Incubation time can be further divided into dead time ($T_1$), the time for the precursor to travel from the source chamber to the reaction chamber, and the time for the first nucleation event to occur ($T_2$). During the dead time ($T_1$), the Au and Au-Ag parts of the substrate remain inert in terms of germination and nucleation because there is no Ge present. However, on the Au-Ag-Ge side, ternary eutectic melt formation can initiate due to the presence of the Ge reaction

layer, thus effectively reducing the dead time ($T_1$). Importantly, on the Au and Au-Ag side: $T_N = T_1 + T_2$, hence, $T = (T_1 + T_2) + T_G$. The Au-Ag side will have a lower $T_2$ value, *i.e* the actual nucleation time; because of the lower equilibrium concentration and faster nucleation of Ge at the TPB with the Au-Ag growth promoter. On the Au-Ag-Ge side, $T_N = T_2$ (dead time $T_1$ is near to zero due to the presence Ge) and so $T = T_2 + T_G$. In other words, single nucleation events take longer on the film sections without the Ge layers because of the added dead time ($T_1$). This added dead time results in a lowering of the effective nanowire growth time ($T_G$) in the film parts without the Ge reaction layer as the total growth time ($T$) remains fixed. Although beyond our capability to compare the timescale of single crystallisation events on each section of a 3-part substrate, a 25 min time interval (the growth time in our experiments) is enough to compare multiple nucleation events in the Au, Au-Ag and Au-Ag-Ge films, which contribute together in the nanowire growth process.[24]

Figure 5(b) presents Ge nanowire lengths as a function of diameter for the Au and $Au_{0.75}Ag_{0.25}$ nanoparticles deposited on Ge films. These measurements were performed on an SEM fitted with a scanning transmission electron microscopy (STEM) detector. Due to the entangled mesh of nanowires on the substrate following nanowire synthesis, accurate diameter and length measurements were not possible. Consequently, nanowires were dispersed in isopropanol and drop-cast onto lacey carbon grids for analysis. The low magnification capabilities of the SEM make it an ideal instrument to measure nanowire lengths and diameters using a STEM detector (figure S6 in the Supporting Information shows how this technique was employed to measure nanowire dimensions for diameter-dependent studies). Figure S6 reveals isolated nanowires from which length and diameter measurements were relatively easy to determine. The sonication time was low (about 5 s) in order to prevent nanowires breaking apart before they were dispersed onto TEM grids, as this can be a common source of error with this procedure. Additionally, length and diameter measurements were only undertaken on nanowires that contained particles at their tips. The length vs diameter data

plotted in figure 5(b), show that the mean nanowire lengths decreased progressively with diameter, with nanowires grown from the $Au_{0.75}Ag_{0.25}$ seeds yielding longer nanowires than those grown from the Au seeds over a similar diameter range. Diameter-dependent nanowires lengths can be explained by the Gibbs-Thomson effect, which provides a relationship between the curvature of the alloy particle surface and its chemical potential [32, 35]. As the difference in the chemical potential between the seed and the nanowire is what governs Ge supersaturation in the eutectic seed and thus the driving force behind nanowire growth, an understanding of how the Gibbs-Thomson relationship affects Ge nanowire growth using the Au-Ge binary and Au-Ag-Ge ternary alloy systems is important. The Gibbs-Thomson relationship states that at nanoscale dimensions, the growth velocity becomes diameter dependent according to equation 4 [36]:

$$\Delta\mu = \Delta\mu_0 - \frac{4\Omega\alpha_{vs}}{d} \qquad (4)$$

where $\Delta\mu$ (supersaturation) is the chemical potential difference of Ge in the vapour phase compared to the nanowire, $d$ is the diameter, $\Delta\mu_o$ is the difference between the chemical potentials of Ge at a planar boundary, $\Omega$ is the atomic volume of the semiconductor species and $\alpha$ is the specific free energy of the nanowire surface. Increasing the nanowire diameter causes an overall increase in the supersaturation (according to equation 4) and consequently, an increase in the driving force behind nanowire growth thus producing longer nanowires as shown experimentally in figure 5(b). Also, small diameter nanowires tend to grow slower than large diameter wires due to increased stabilisation of the particle seed as a result of capillary effects [37], resulting in longer lengths for large diameter nanowires, which again is reflected in figure 5(b).

**In-situ temperature TEM studies and calculation of Ge equilibrium concentration**

To confirm the observed length dependence on diameter for Ge nanowires grown from Au-Ge and Au-Ag-Ge alloy systems, and to support the nanowire growth characteristics as a function of Ge equilibrium concentration ($C_{eq}$), in-situ TEM heating experiments were performed on nanowires of varying diameters. The Gibbs-Thomson effect discussed above is summarised in equation (5)[8] below, in terms of Ge solute concentration in nanoscale and bulk equilibrium concentrations:

$$C_n = C_{eq} \exp\left(\frac{4\Omega\alpha}{dkT}\right) \quad (5)$$

where $C_n$ is the diameter dependent Ge equlibrium concentration in the alloy for a nanowire of radial dimension $d$, $C_{eq}$ is the equilibrium concentration for the bulk counterpart. Figure 6(a) shows a TEM image of a Ge nanowire grown from a Au-Ag-Ge ternary alloy catalyst. Figure 6(b) represents the same nanowire after heating to the growth temperature of 465 ºC. The expansion of the liquid-solid interface into the nanowire, as a result of Ge uptake into the seed upon heating, was evident and has previously been demonstrated by Sutter *et al.*[38] Additional TEM images of the in-situ TEM heating of nanowires grown from both Au and $Au_{0.75}Ag_{0.25}$ nanoparticle seeds are presented in the Supporting Information, figure S7. The expansion of the seed particle was used to calculate the equilibrium Ge concentration, $C_{eq}$ in the seed, following the approaches outlined by Sutter *et al.* [27, 28]. This method is outlined in detail in the Supporting Information. Figure 6(c) depicts $C_{eq}$ in the particle tip of the nanowires as a function of nanowire diameter for both the Au-Ge and Au-Ag-Ge systems. The diameter dependence on the nanoscale equilibrium concentration showed a clear increase in the equilibrium Ge atomic fraction ($C_{eq}$) for nanowires with decreasing diameter for both seeds. This increase in $C_{eq}$ leads to a lowering of the supersaturation according to the Givagizov model [32], thus reducing the driving force for nanowire growth and producing shorter nanowires. The

plot shown in figure 6(c) infers a lower equilibrium concentration (higher supersaturation) for the Au-Ag-Ge system compared to a Au-Ge system for a given diameter range, thus supporting the role of a lowered equilibrium concentration in yielding higher nanowire growth rates; observed for nanowires synthesised using a Au-Ag-Ge ternary system. Considering the diameter dependence on the equilibrium concentration, equation (5) gives a theoretical Ge concentration curve as shown by the black (Au-Ag-Ge) and red (Au-Ge) lines in figure 6(c), similar to that obtained by Han *et al.* for the Au-Ga system [9]. The red squares and black hexagons on the plot represent the experimental results for the Au-Ge and Au-Ag-Ge systems respectively. The experimental trend agrees well with the simulated fits for both systems. The discrepancies between the experimental and simulated plots may be due to the difference between simulating spherical particle tips and calculating the Ge concentration from actual hemispherical seeds, as reported by Han *et al.* [9]. The diameter-dependent growth rate shown in figure 5(b) and the size-dependent equilibrium concentration displayed in figure 6(c) can both be explained by the Gibbs-Thomson effect.[8] The in-situ TEM heating experiments showing lower nanoscale equilibrium concentration for larger diameter nanowires supports the observation of diameter-dependent nanowire growth rates, as shown in figure 5.

## Conclusion

To conclude, we report for the first time the simultaneous manipulation of the Ge solute concentration ($C$) and the equilibrium concentration ($C_{eq}$) in a Au-Ag-Ge ternary alloy system, to produce high quality Ge nanowires and enhance the nanowire growth kinetics. Nanowire lengths were maximised with the addition of Ag and Ge films to a Au-coated substrate, keeping all other growth constraints constant. A bi-modal diameter distribution was observed for nanowires grown from the Au-Ag-Ge tri-layer film and was subsequently eliminated through the combination of colloidal $Au_{0.75}Ag_{0.25}$ nanoparticle seeds and a Ge reaction layer. Size-dependent properties of Ge nanowires seeded from Au and $Au_{0.75}Ag_{0.25}$ nanoparticles were explained and compared through the

Gibbs-Thompson relationship. Finally, in-situ TEM heating experiments were conducted on the nanowires post-growth to support the size dependent growth kinetics observed for both Au-Ge binary and Au-Ag-Ge ternary alloy seeds used to catalyse Ge nanowire growth. The combination of adding a Ge film to increase the solute concentration in the Au-Ge system, while simultaneously reducing the equilibrium concentration through the incorporation of Ag, may yield a highly ideal growth scenario in future work when combined with other growth kinetic influencing parameters such as temperature and pressure.

**Acknowledgements**

We acknowledge financial support from the Irish Research Council and Science Foundation Ireland (Grants: 09/SIRG/I1621 and 09/IN.1/I2602).

**Supporting Information.** Schematic and photograph illustrating the composition of the 3-part substrate, additional SEM images comparing the lengths of Ge nanowires, further in-situ and high resolution TEM images showing the particle seed expansion as well as confirming the nanowire crystallinity and orientation and STEM, EDX and uv-visible spectroscopic analysis of the particle seeds.

## References


1. J. Andzane, N. Petkov, A. I. Livshits, J. J. Boland, J. D. Holmes and D. Erts, *Nano Lett.* 2009, **9**, 1824.
2. K. J. Ziegler, D. M. Lyons, J. D. Holmes, D. Erts, B. Polyakov, H. Olin, K. Svensson and E. Olsson, *Appl. Phys. Lett.* 2004, **84**, 4074.
3. A. M. Chockla, K. C. Klavetter, C. B. Mullins and B. A. Korgel, *ACS Appl. Mater. Inter.* 2012, **4**, 4658.
4. M. H. Seo, M. Park, K. T. Lee, K. Kim, J. Kim and J. Cho, *Energy Environ. Sci.* 2011, **4**, 425.
5. C. K. Chan, X. F. Zhang and Y. Cui, *Nano Lett.* 2008, **8**, 307.
6. T. Burchhart, A. Lugstein, Y. J. Hyun, G. Hochleitner and E. Bertagnolli, *Nano Lett.* 2009, **9**, 3739.
7. B Lewis and J. S. Anderson, *Nucleation and Growth of Thin Films*. Academic, New York: 1978.
8. S. A. Dayeh and S. Picraux, *Nano Lett.* 2010, **10**, 4032.
9. N. Han, F. Wang, J. J. Hou, S. P. Yip, H. Lin, M. Fang, F. Xiu, X. Shi, T. F. Hung and J. C. Ho, *Cryst. Growth. Des.* 2012, **12,** 6243.
10. C. O'Regan, S. Biswas, C. O'Kelly, S. J. Jung, J. J. Boland, N. Petkov and J. D. Holmes, *Chem. Mater.* 2013, **25**, 3096.
11. D. E. Perea, N. Li, R. M. Dickerson, A. Misra and S. Picraux, *Nano Lett.* 2011, **11**, 3117.
12. S. Biswas, A. Singha, M. A. Morris and J. D. Holmes, *Nano Lett.* 2012, **12**, 5654.
13. S. Biswas, C. O'Regan, N. Petkov, M. A. Morris and J. D. Holmes, *Nano Lett.* 2013, **13**, 4044.
14. Y.-C. Chou, C.-Y. Wen, M. C. Reuter, D. Su, E. A. Stach and F. M. Ross, *ACS Nano* 2012, **6**, 6407.
15. C. Y. Wen, M. C. Reuter, J. Bruley, J. Tersoff, S. Kodambaka, E. A. Stach and F. M. Ross, *Science* 2009, **326**, 1247.
16. J. Wang, Y. J. Liu, C. V. Tang, L. B. Liu, H. Y. Zhou and Z. P. Jin, *Thermochim. Acta.* 2011, **512**, 240.
17. J. Wang, C. Leinenbach and M. Roth, *J. Alloy. Compd.* 2009, **481**, 830.
18. J. Wang, C. Leinenbach and M. Roth, *J. Alloy. Compd.* 2009, **485**, 577.
19. S. Jin, L. I. Duarte, G. Huang and C. Leinenbach, *Monatsh. Chem.* 2012, **143**, 1263.
20. E. Sutter and P. Sutter, *Appl. Phys. A-Mater.* 2010, **99**, 217.
21. E. J. Schwalbach and P. W. Voorhees, *Nano Lett.* 2008, **8**, 3739.
22. B. J. Kim, C. Y. Wen, J. Tersoff, M. C. Reuter, E. A. Stach and F. M. Ross, *Nano Lett.* 2012, **12**, 5867.
23. A. Gamalski, J. Tersoff, R. Sharma, C. Ducati and S. Hofmann, *Phys. Rev. Lett.* 2012, **108**, 255702.
24. A. Gamalski, C. Ducati and S. Hofmann, *J. Phys. Chem. C* 2011, **115**, 4413.
25. F. M. Ross, *Rep. Prog. Phys.* 2010, **73**, 114501.
26. S. Kodambaka, J. Tersoff, M. Reuter and F. Ross, *Science* 2007, **316**, 729.
27. E. A. Sutter and P. W. Sutter, *ACS Nano* 2010, **4**, 4943.
28. E. Sutter and P. Sutter, *Nano Lett.* 2008, **8**, 411.
29. S. Liu, G. Chen, P. N. Prasad and M. T. Swihart, *Chem. Mater.* 2011, **23**, 4098.
30. H. Okamoto and T. Massalski, *Bull. Alloy. Phase. Diagr.* 1984, **5**, 601.
31. G. Borzone, S. Hassam and J. Bros, *Metall. Mater. Trans. A* 1989, **20**, 2167.
32. E. I. Givargizov, *J. Cryst. Growth* 1975, **31**, 20.
33. V. Schmidt, J. V. Wittemann, S. Senz and U. Gösele, *Adv. Mater.* 2009, **21**, 2681.
34. O. Lotty, R. Hobbs, C. O'Regan, J. Hlina, C. Marschner, C. O'Dwyer, N. Petkov and J. D. Holmes, *Chem. Mater.* 2012, **25**, 215.
35. R. Laocharoensuk, K. Palaniappan, N. A. Smith, R. M. Dickerson, D. J. Werder, J. K. Baldwin and J. A. Hollingsworth, *Nature Nanotech.* 2013, **8**, 660.
36. E. I. Givargizov, *Highly anisotropic crystals*. D Reidel Pub Co: 1987; Vol. 3.
37. V. C. Holmberg, M. G. Panthani and B. A. Korgel, *Science* 2009, **326**, 405.
38. E. Sutter and P. Sutter, *Nanotechnology* 2011, **22**, 295605.

## Figures and Tables

**Table 1.** Summary of lengths and growth rates of Ge nanowires

| | Au film | Au-Ag film | Au-Ag-Ge film (4 nm Ge) | Au-Ag-Ge film (6 nm Ge) | AuNPs on $Si/SiO_2$ (no Ge film) | Au NPs on 6 nm Ge film | $Au_{0.75}Ag_{0.25}$ NPs on 6 nm Ge film |
|---|---|---|---|---|---|---|---|
| Length (μm) | 2.0 ± 0.9 | 5.0 ± 4.2 | 5.7 ± 2.3 | 7.3 ± 4.3 | 2.3 ± 0.9 | 4.4 ± 1.7 | 8.7 ± 5.2 |
| Growth Rate ($\times 10^{-3}$ μm $s^{-1}$) | 1.1 ± 0.9 | 2.7 ± 4.2 | 3.2 ± 2.3 | 4.1 ± 4.3 | 1.3 ± 0.9 | 2.4 ± 1.7 | 4.8 ± 5.2 |

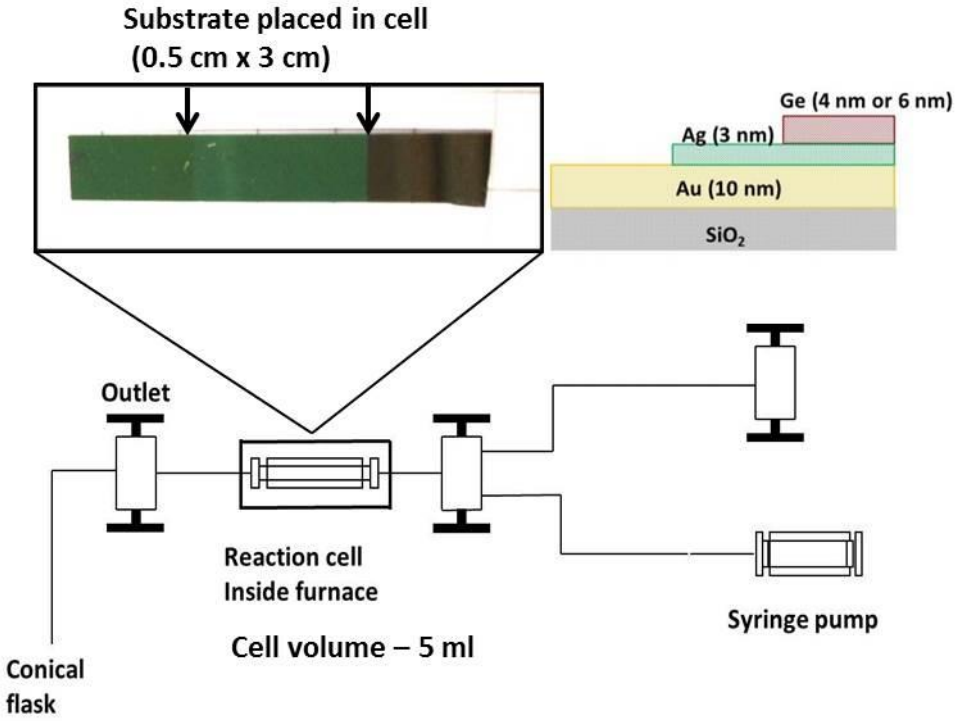


**Figure 1.** Schematic of the liquid-injection CVD experimental set-up used to synthesise Ge nanowires. The various layers of the 3-part substrate are shown in the top-down photograph and cross-sectional schematic. The top-down photograph clearly shows the 3 parts of the substrate with the interface between each section highlighted by the black arrows. The left section is Au, the middle section is Au-Ag and the section on the right is Au-Ag-Ge. This also corresponds to the cross-sectional schematic.

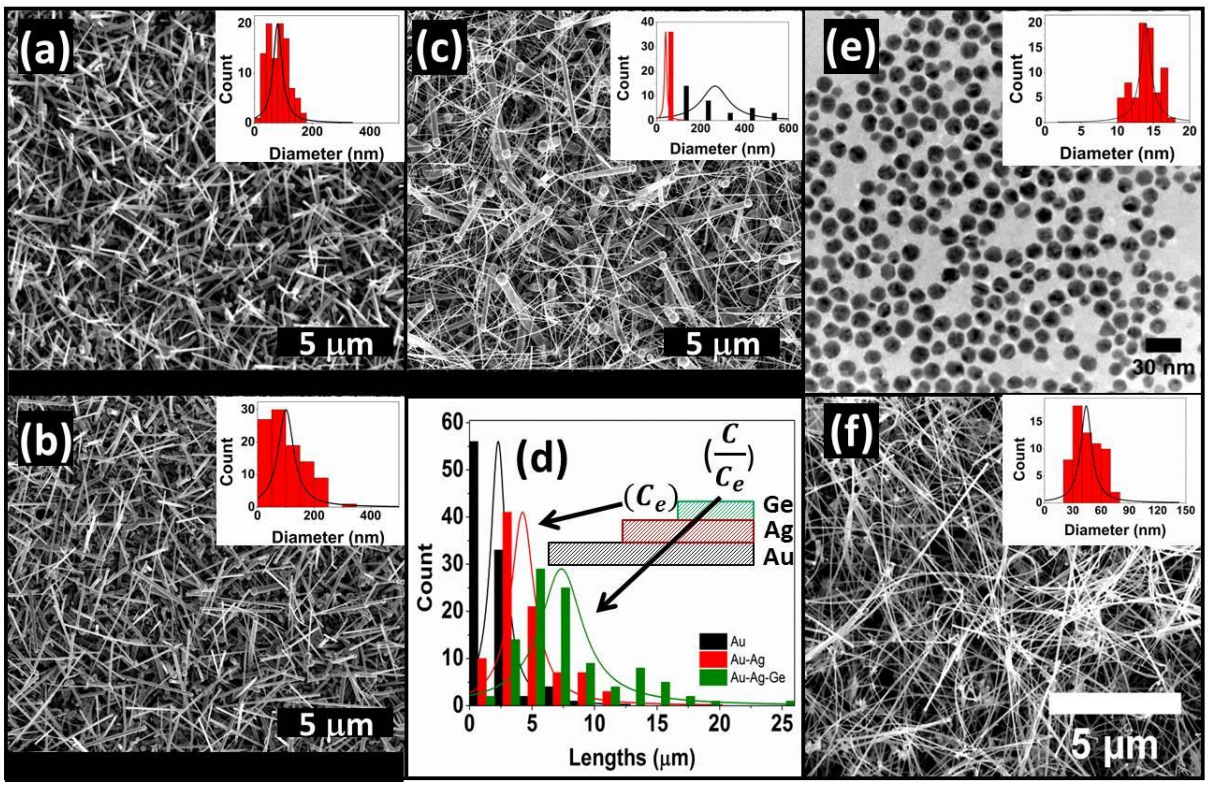


**Figure 2.** SEM images of Ge nanowires grown using a 3-part substrate. (a) Ge nanowires grown on the Au part of the 3-part substrate. (b) Ge nanowires grown on the Au-Ag bi-layer part of the 3-part substrate. (c) Ge nanowires grown on the Au-Ag-Ge part of the 3-part substrate. (d) Nanowire length distributions from the Au film, Au-Ag bi-layer and Au-Ag-Ge tri-layer showing how the mean nanowire length increases on proceeding from the Au film to the Au-Ag bi-layer and finally, to the Au-Ag-Ge tri-layer. The inset illustrates how each part of the substrate influences the growth kinetics, with the addition of Ag reducing $C_{eq}$ in the bi-layer and the addition of Ge to Au-Ag increasing the solute concentration in the tri-layer. (e) TEM image of $Au_{0.75}Ag_{0.25}$ nanoparticles dispersed on a lacey carbon grid with a mean diameter is 13.9 ± 1.9 nm. (f) SEM image of Ge nanowires grown from the $Au_{0.75}Ag_{0.25}$ nanoparticles shown in (e), with a mean diameter is 44 ± 14. Insets in (a), (b), (c), (e) and (f) are diameter distributions confirming the presence ((c)) or absence ((a), (b), (e) and (f)) of a bi-modal diameter regime.

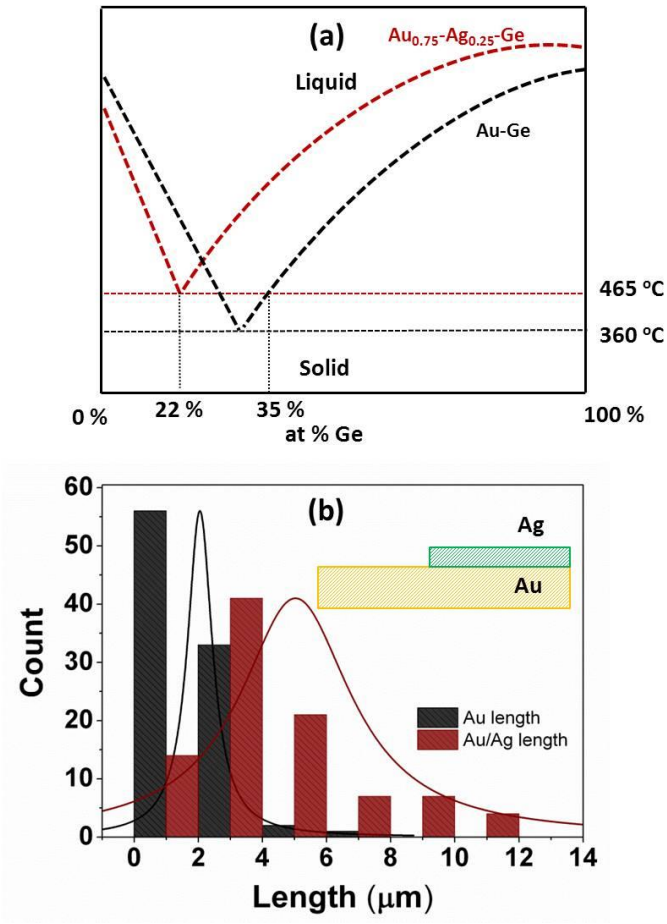


**Figure 3.** Diameter distributions highlighting the difference in lengths of nanowires grown from a Au film and a Au-Ge bilayer. (a) Phase diagram showing the shift in equilibrium concentration in the Au-Ag-Ge ternary alloy system when compared with the Au-Ge binary system. (b) Length distribution data comparing the lengths between nanowires grown from a Au film and a Au-Ag bi-layer.

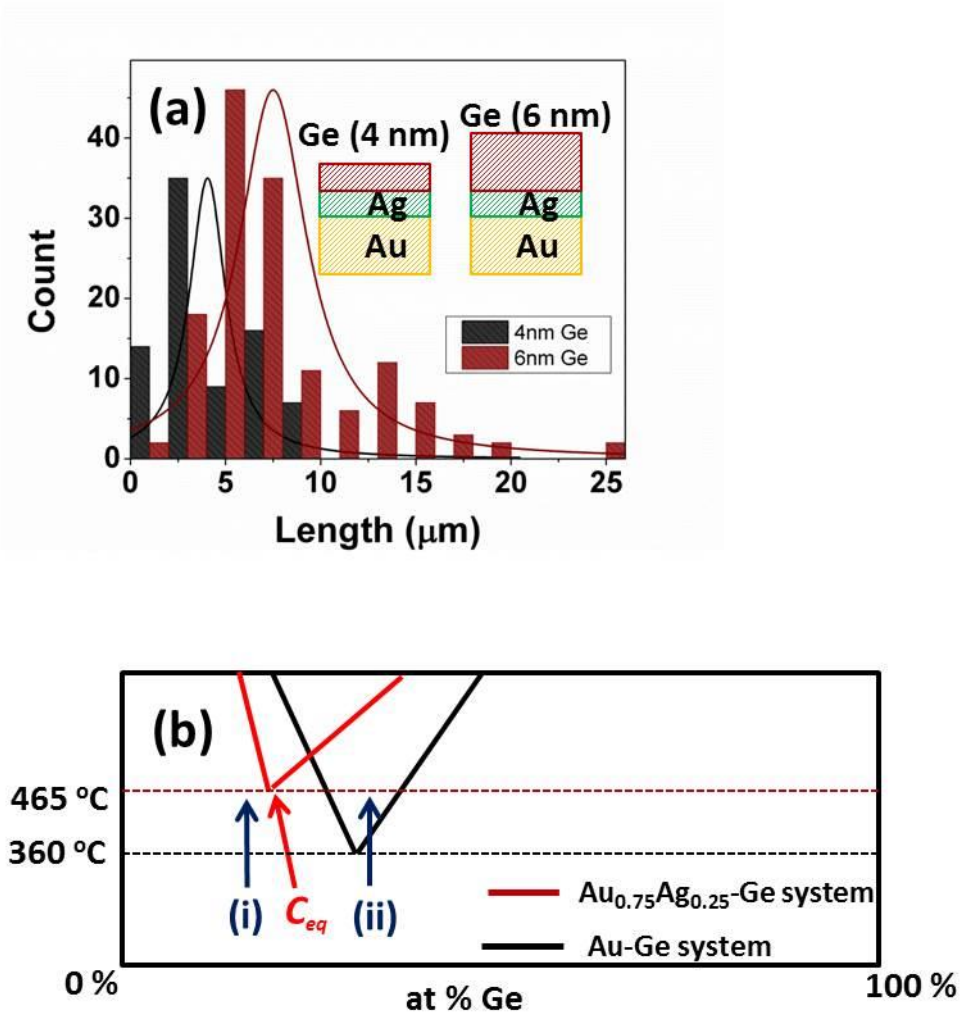


**Figure 4.** The influence of Ge film thickness on nanowire growth. (a) Length distribution data for nanowires for Ge nanowires grown from 4 nm and 6 nm Ge films. (b) Magnified schematic of the eutectic region of the phase diagram in figure 3(a). The black curve represents the liquidus for the Au-Ge binary alloy system at the eutectic temperature of 360 ºC and equilibrium composition, $C_{eq}$ of 28 %. The red curve represents the shift in the liquidus to a $C_{eq}$ of 22 % Ge in Au when Ag is added to the system, forming a Au-Ag-Ge ternary alloy.

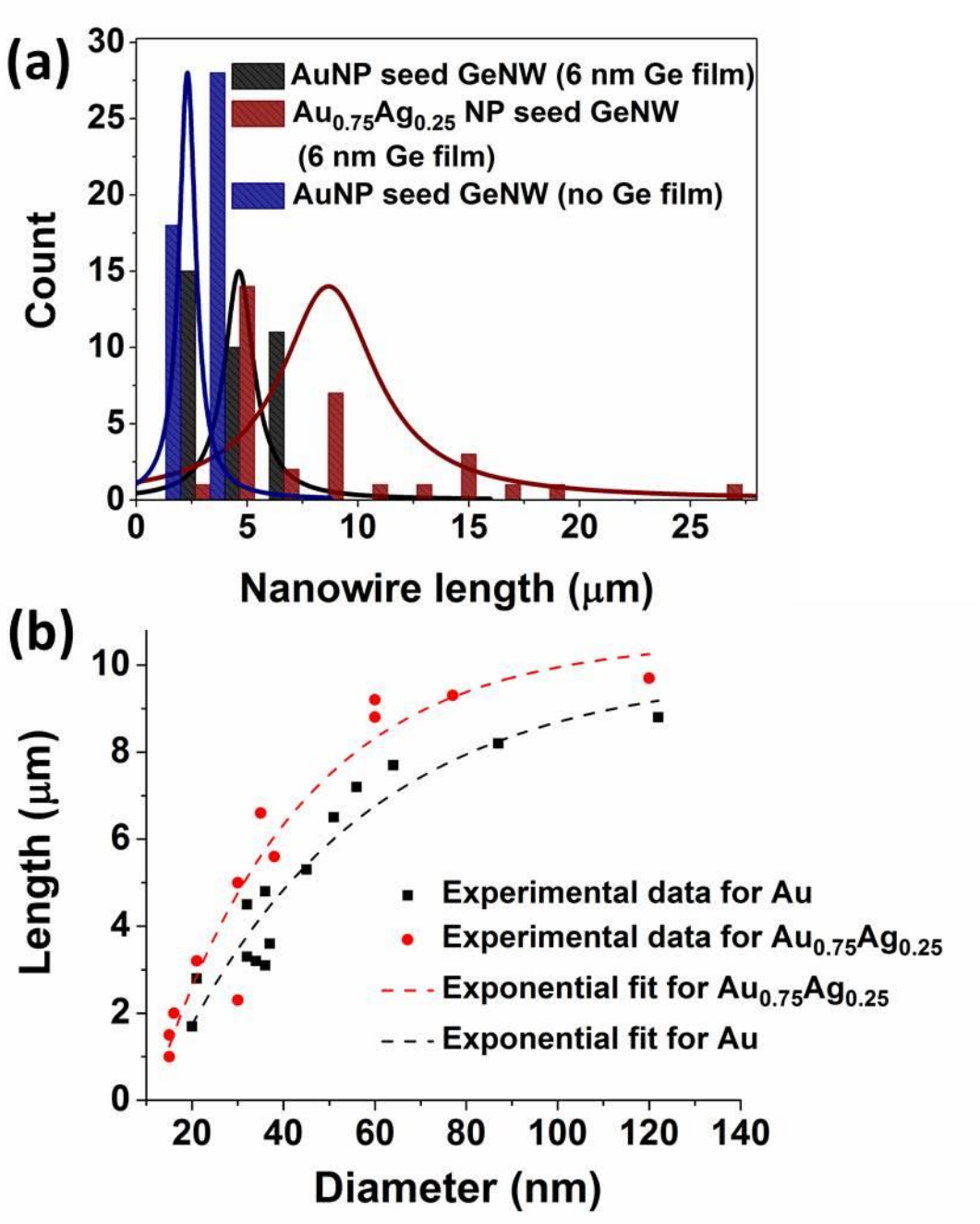


**Figure 5.** Plots of nanowire length vs growth rate showing the applicability of the Gibbs-Thompson effect. (a) Length distribution curves comparing the lengths of Ge nanowires grown from Au and $Au_{0.75}Ag_{0.25}$ nanoparticles. (b) Plot of nanowire length as a function of diameter for nanowires grown from Au and $Au_{0.75}Ag_{0.25}$ nanoparticles.

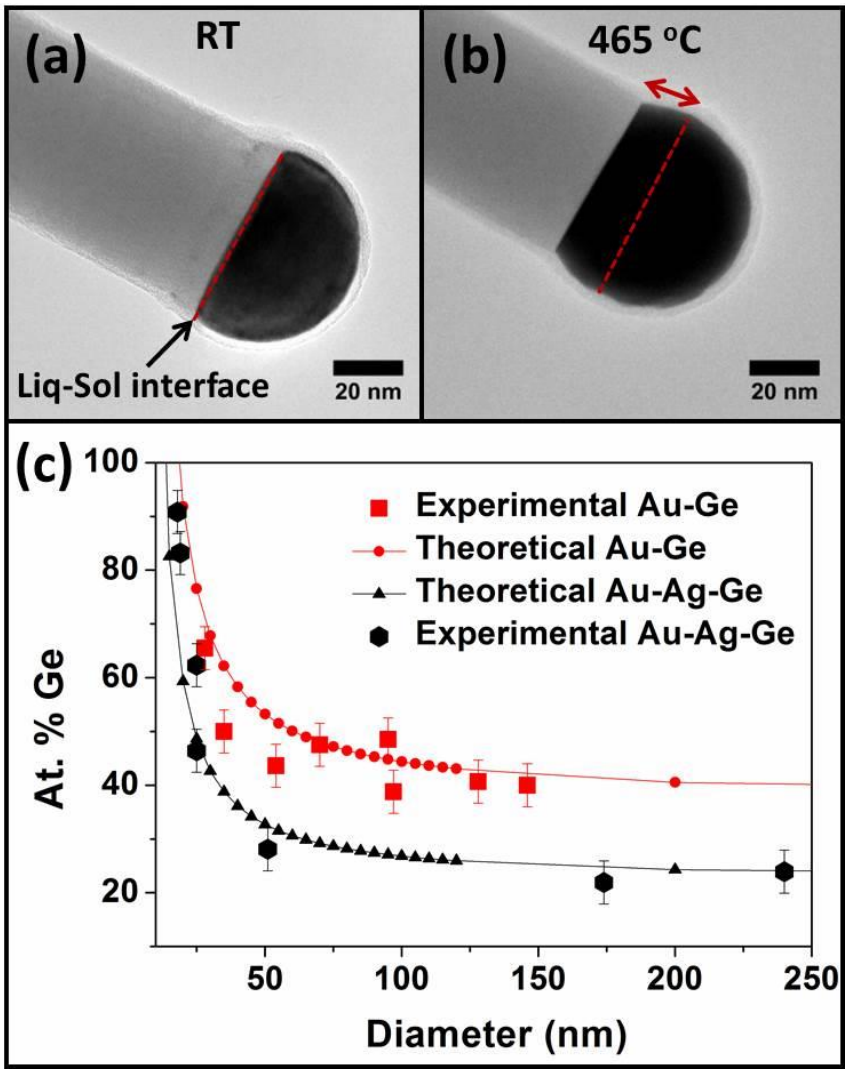


**Figure 6.** Data obtained from in-situ TEM heating of Ge nanowires grown from $Au_{0.75}Ag_{0.25}$ and Au nanoparticle seeds. (a) TEM image of a $Au_{0.75}Ag_{0.25}$ nanoparticle seeded Ge nanowire at room temperature. (b) TEM image of the same nanowire after heating to the growth temperature of 465 ºC. (a) and (b) show the expansion of the nanowire liquid-solid interface as a result of Ge uptake into the seed. (c) Plot of the equilibrium Ge atomic % calculated from particle expansion as a function of nanowire diameter for the Au-Ge (red squares) and Au-Ag-Ge (black hexagons) alloy systems. Simulated curves for the experimental data for the Au-Ge (red line) and Au-Ag-Ge (black line) of the supersaturation of Ge in Au and $Au_{0.75}Ag_{0.25}$ nanoparticles are included.

**Table of Contents Figure**

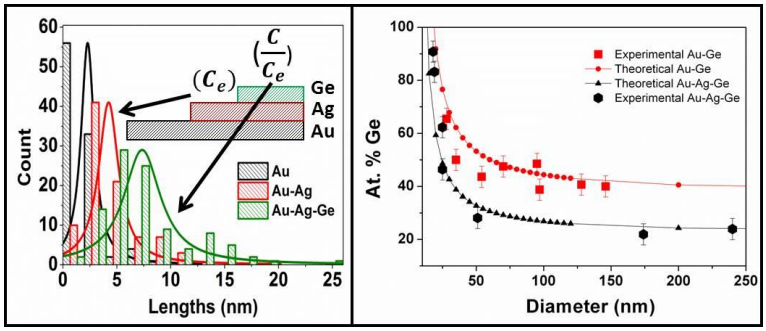


We report the simultaneous manipulation of both solute and equilibrium concentration of Ge to synthesise high aspect-ratio Ge nanowires.